Low-dimensional emissive states in non-stoichiometric methylammonium lead halide perovskites

Benjamin G. Freestone[1], Joel A. Smith[1], Giacomo Piana[2], Rachel C. Kilbride[1], Andrew J. Parnell[1], Luca Sortino[1], David M. Coles[1], Orianna B. Ball[1], Natalia Martsinovich[3], Courtney Thompson[3], Tarek I. Alanazi[1], Onkar S. Game[1], Alexander I. Tartakovskii[1], Pavlos Lagoudakis[2] and David G. Lidzey[1]

[1] *Department of Physics and Astronomy, University of Sheffield, Sheffield, S3 7RH, U.K.*

[2] *Department of Physics and Astronomy, University of Southampton, SO17 1BJ, U.K.*

[3] *Department of Chemistry, University of Sheffield, S3 7RH, U.K.*

Supplementary Information

Tables

Table S1: Energy dispersive X-ray analysis of films produced from MAI:$PbCl_2$ stoichiometries of 2.5:1, 3:1 and 3.5:1.
Table S2: Tabulated values of peaks expected for $MAPbI_3$, PbI_2, MAI and observed LDP peaks up to Q = 1.2 $Å^{-1}$.
Table S3: Calculated and experimental lattice parameters for PBEsol and C09 functional calculations on $MA_4Pb_3I_{10}$ and $GAMA_3Pb_3I_{10}$.

Figures

Figure S1: Effect of HI addition on crystallography of 3:1 films and GIWAXS comparison of excess MAI and HI films.
Figure S2: 1H and 13C NMR spectroscopy of dissolved films with various stoichiometries.
Figure S3: Representative crystal structure of the $GA(MA)_3Pb_3I_{10}$ DJ/RPP hybrid (ACI) phase
Figure S4: Simulated pXRD and representative crystal structures of C09 $MA_4Pb_3I_{10}$ DJ/RPP-like phase.
Figure S5: Grazing incidence wide-angle X-ray scattering (GIWAXS) patterns and depth profiles of perovskite films 4:1 air annealed and after exposure to high humidity
Figure S6: Low-temperature (11 K) absorption spectrum for a stoichiometric (3:1) perovskite film.
Figure S7: PL emission spectra for air annealed 3.5:1 and N2 glovebox annealed 4:1 samples plotted on a log-scale at room and low temperature
Figure S8: Temperature-dependant photoluminescence emission series for 3.5:1 air annealed film on hole-quenching ITO/PEDOT:PSS substrate and 4:1 air-annealed film.
Figure S9: Low-temperature PL comparison of 3.5:1 and 4:1 excess MAI perovskite films
Figure S10: Emergence of low dimensional absorption features at low temperature.

Precursor molar ratio [MAI:$PbCl_2$]	Element	Formula	Mass [%]	Atom [%]
2.5:1	C	41.23	89.21	0.21
	Cl	0.36	0.268	0.19
	I	39.00	8.26	2.17
	Pb	18.48	2.33	1.08
3:1	C	4.97	37.65	0.01
	Cl	0	0	0
	I	74.31	53.25	0.30
	Pb	20.72	9.10	0.14
3.5:1	C	6.417	44.02	0.02
	Cl	0	0	0
	I	74.60	48.43	0.43
	Pb	18.98	7.55	0.19

Table S1: Energy dispersive X-ray analysis of films produced from MAI:$PbCl_2$ stoichiometries of 2.5:1, 3:1 and 3.5:1, where values are averages of up to 5 large area scans at different locations on the films. In both 3:1 and 3.5:1 there is no detectable Cl, indicating a completion process whereby additional MA & Cl assists during film formation but remnant material above stoichiometry is removed during annealing (see "Phase Analysis" section). Carbon detection here is thought to be inaccurate due to the nature of the technique, which prevents precise determination of the stoichiometry of the LDP structures formed.

Expected peak origin	Q (Å^{-1})	2θ calculated for λ = 1.5406 Å	m (order of reflection)	d-spacing (Å)
$MAPbI_3$ (110)/LDP	1.00-1.02*	14.16	1	6.28
PbI_2/LDP	0.89	12.53	1	7.06
MAI	0.71	9.99	1	8.85
Observed LDP peaks	0.29	4.08	1	21.67
	0.59	8.32	2	10.65
	0.88	12.39	3	7.14
	1.14	16.08	4	5.51

Table S2: Tabulated values of peaks expected for $MAPbI_3$, PbI_2, MAI and observed LDP peaks up to Q = 1.2 Å^{-1} which do not correspond with other expected structures. PbI_2 peak at 0.89 coincides closely with LDP peak at Q ≈ 0.88 Å^{-1} and (110) $MAPbI_3$ peak measured at Q ≈ 1.0 Å^{-1} may be related to both 3D perovskite and LDP structures. The Bragg condition for constructive interference is given by: $2d\ sin\ \theta = m\lambda$. * We note a small shift of this reflection in both the additional MAI and HI cases as seen in Figure 2c and Figure S1a.

Phase	Method	a	b	c	z (height)
$GAMA_3Pb_3I_{10}$	Expt[1]	6.35	6.22		21.99
	PBEsol	6.42	6.24	22.98	21.86
	C09	6.38	6.22	22.60	21.55
$MA_4Pb_3I_{10}$	Expt	6.28	6.28		21.67
	PBEsol	6.33	6.29	23.85	22.81
	C09	6.37	6.14	22.86	21.77

Table S3: Lattice parameters and layer spacings for n = 3 ACI perovskite as previously reported[1] and possible LDP $MA_4Pb_3I_{10}$. DFT modelling using C09 and PBEsol functionals was performed for the crystal structure previously reported for $GAMA_3Pb_3I_{10}$ and by replacing all GA cations with MA. Full methodology is detailed in the Experimental section.

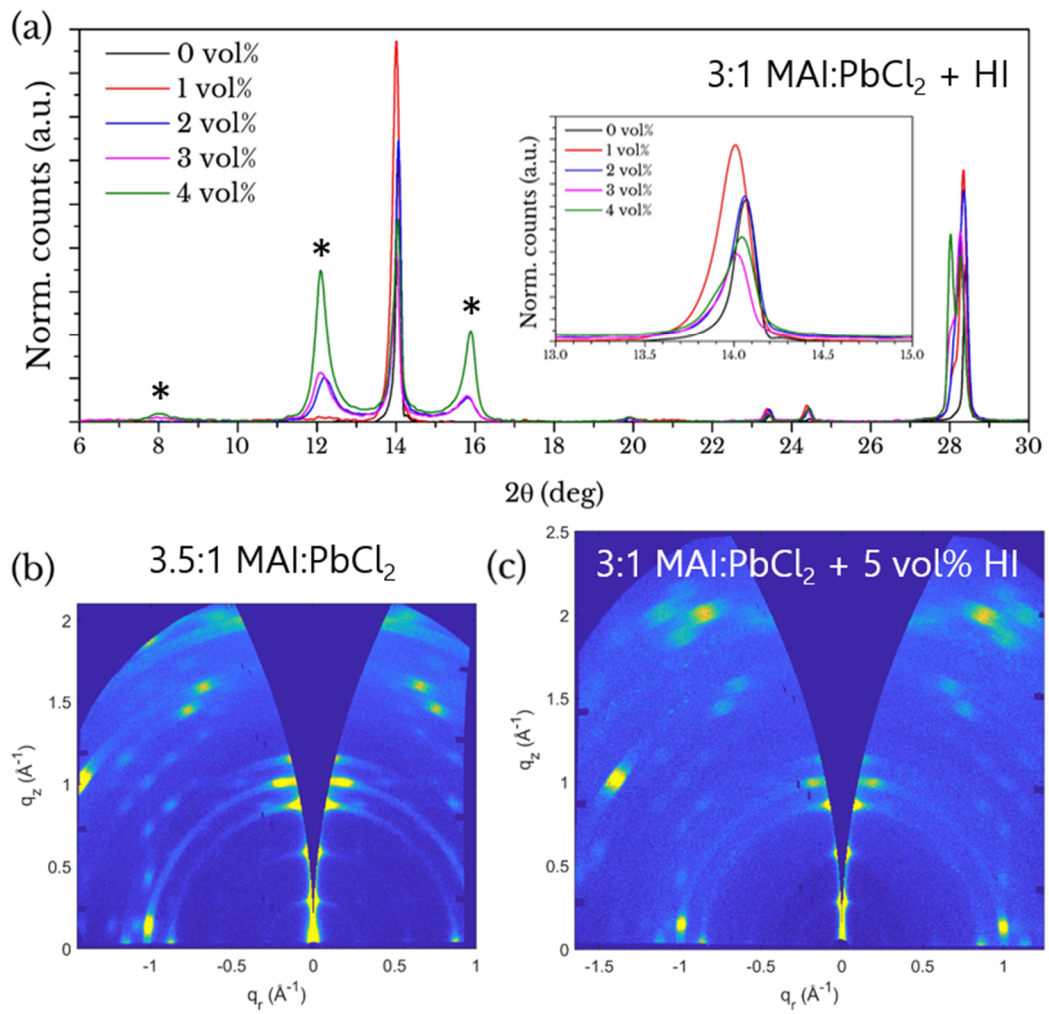

Figure S1: (a) XRD patterns of 3:1 MAI:$PbCl_2$ samples with volumetric addition of hydroiodic acid. Peaks denoted with * correlate with those identified in MAI excess samples as shown in Figure 2. Inset is detail of the scattering typically associated with the (110) $MAPbI_3$ *I4/mcm* lattice vector, showing a shift to higher scattering angles upon addition of HI, suggesting a compression of the lattice if from $MAPbI_3$ perovskite phase. (b) GIWAXS scattering pattern from a 3.5:1 MAI:$PbCl_2$ excess organic sample (with no HI addition), as shown n Figure 2b. (c) 3:1 sample which by inspection with part (b) shows almost identical scattering features and Bragg spots (scales adjusted for ease of comparison).

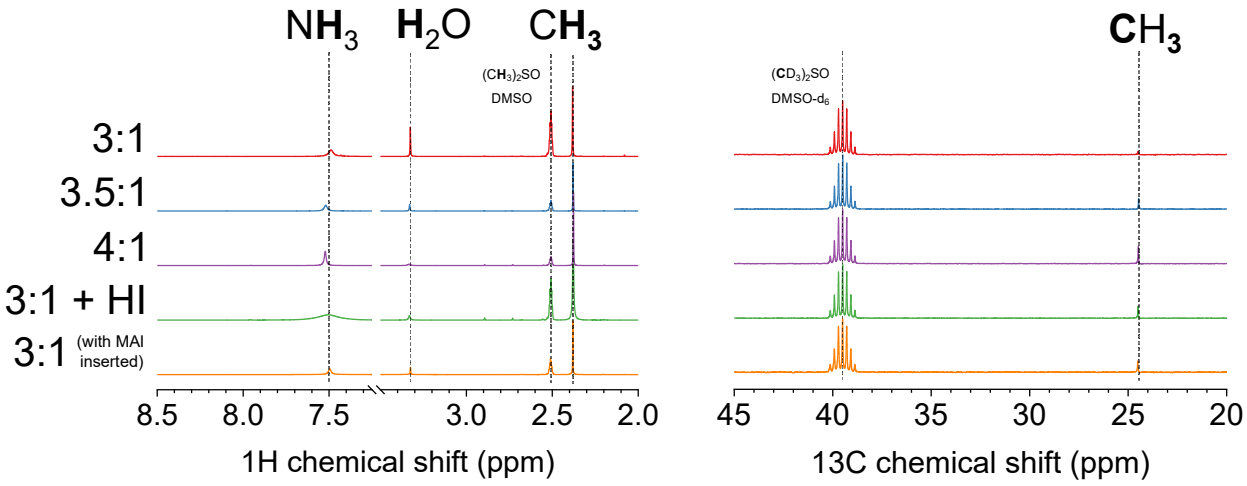

Figure S2: Solution state (a) 1H NMR and (b) 13C NMR of various stoichiometric and non-stoichiometric perovskite films which were re-dissolved in DMSO-d_6. In part (a) we see similar spectra for each composition, with characteristic a C**H**$_3$ peak at δ = 2.38 ppm and N**H**$_3$ at ~δ = 7.5 ppm. In the 13C spectra, only one carbon-containing species is observed. To confirm that these peaks correlate with MAI, we dissolved pure MAI in DMSO-d_6 and placed it inside an inner capillary within the NMR tube for the 3:1 sample (to avoid chemical interaction) and confirm that the peaks observed in all samples match with those observed for CH_3NH_3I. There is some variation in the N**H**$_3$ peak position: 3:1 at δ = 7.49 ppm, 3.5:1 at δ = 7.52 ppm, 3:1 + 5%HI at δ = 7.51 ppm and 4:1 at δ = 7.52 ppm. The 3:1 + 5%HI N**H**$_3$ peak shows significant exchange broadening, and small DMF peaks (assumed to be from GB contamination) are seen at δ = 2.73, 2.89 and 7.95 ppm to some extent in all samples.

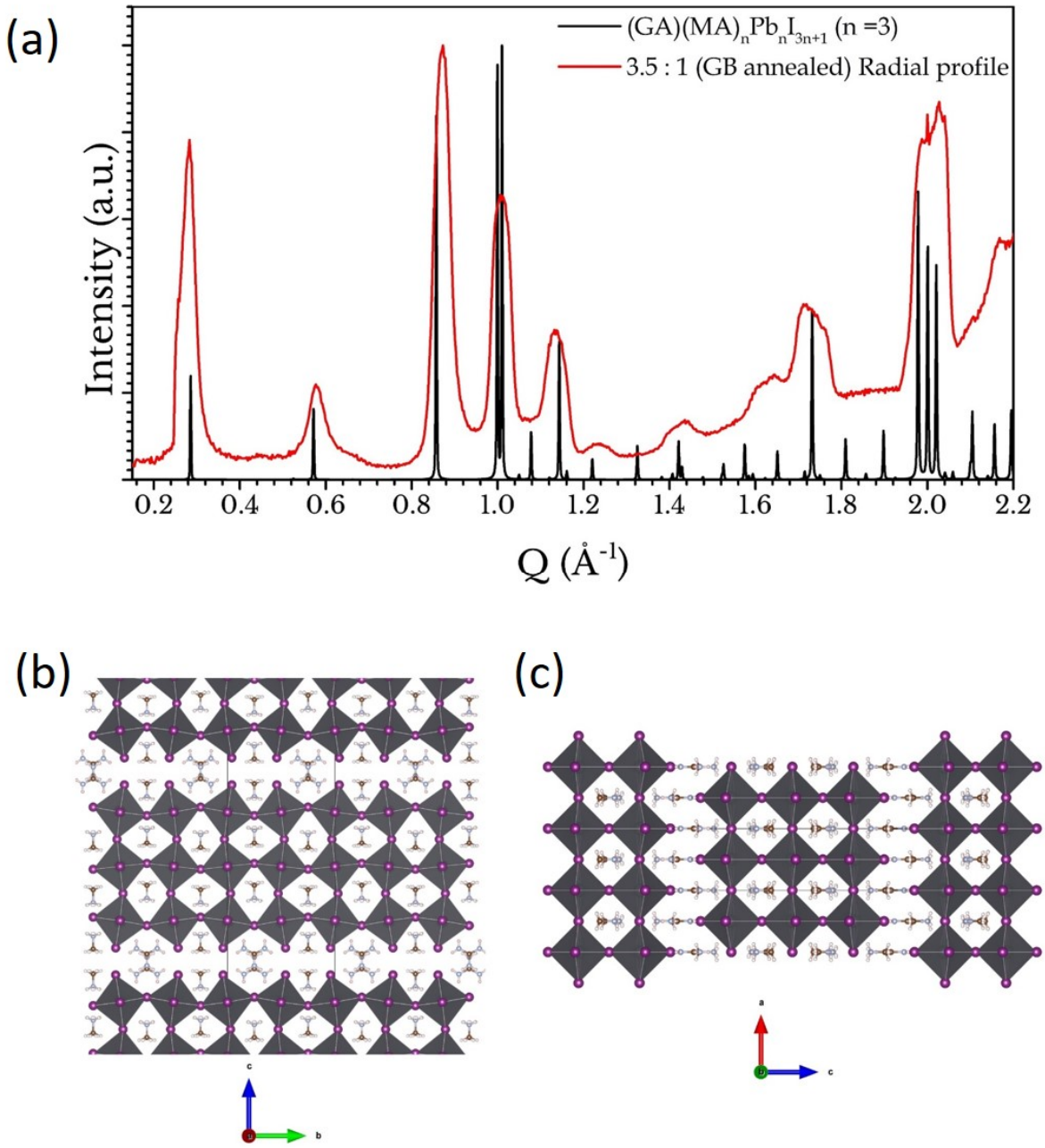

Figure S3: (a) Radially integrated GIWAXS pattern from a 3.5:1 GB annealed sample (red line) plotted together with a powder-XRD simulation using the CIF file for an n=3 ACI perovskite[1] (black lines) provided in reference. Crystal representations of the $GA(MA)_3Pb_3I_{10}$ perovskite indicating no translation along the b-axis (b) and a 1/2 translation in the a-axis (c). The powder-XRD simulation (part (a)) and figures shown in parts (b) and (c) were modelled in the Vesta crystallographic analysis software.[2] The axis label underneath parts (b) and (c) represent the vectors along the a-axis (red), b-axis (green) and c-axis (blue).

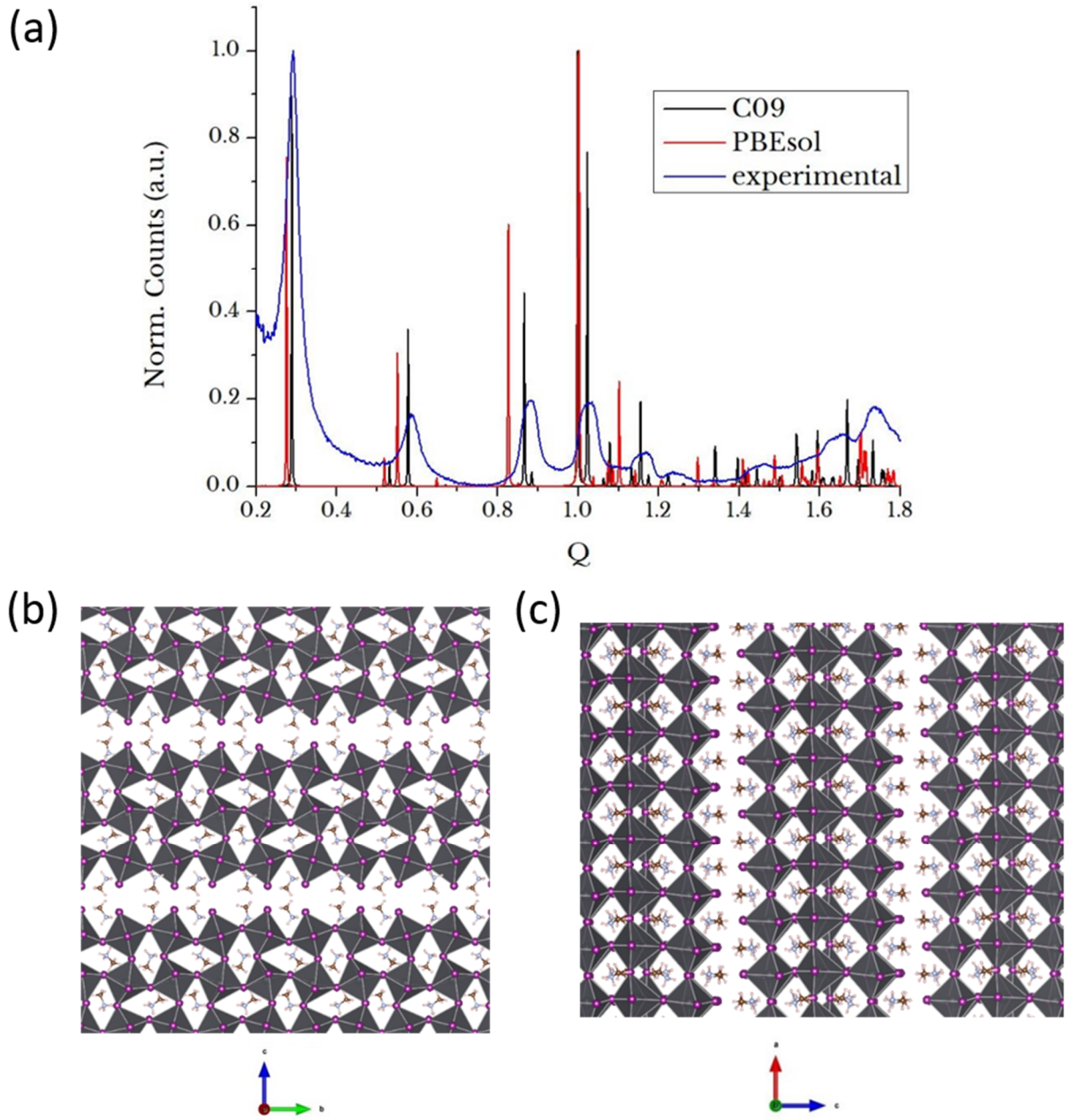

Figure S4: (a) Radially integrated GIWAXS pattern from a 4:1 GB annealed sample (blue line) plotted together with simulated powder XRD from $MA_4Pb_3I_{10}$ phase relaxed using two DFT functionals; PBEsol and C09. Crystallographic representations of the C09 relaxed structure along (b) the a-axis and (c) the b-axis. As with Figure S3 in this structure there is no translation along the b-axis and a translation by 1/2 of the lattice parameter (lateral offset) in the a-axis. The powder-XRD simulation in part (a) and figures shown in parts (b, c) were modelled in the Vesta crystallographic analysis software.[2] Axis labels shown under the crystal structures represent the vectors along the a-axis (red), b-axis (green) and c-axis (blue).

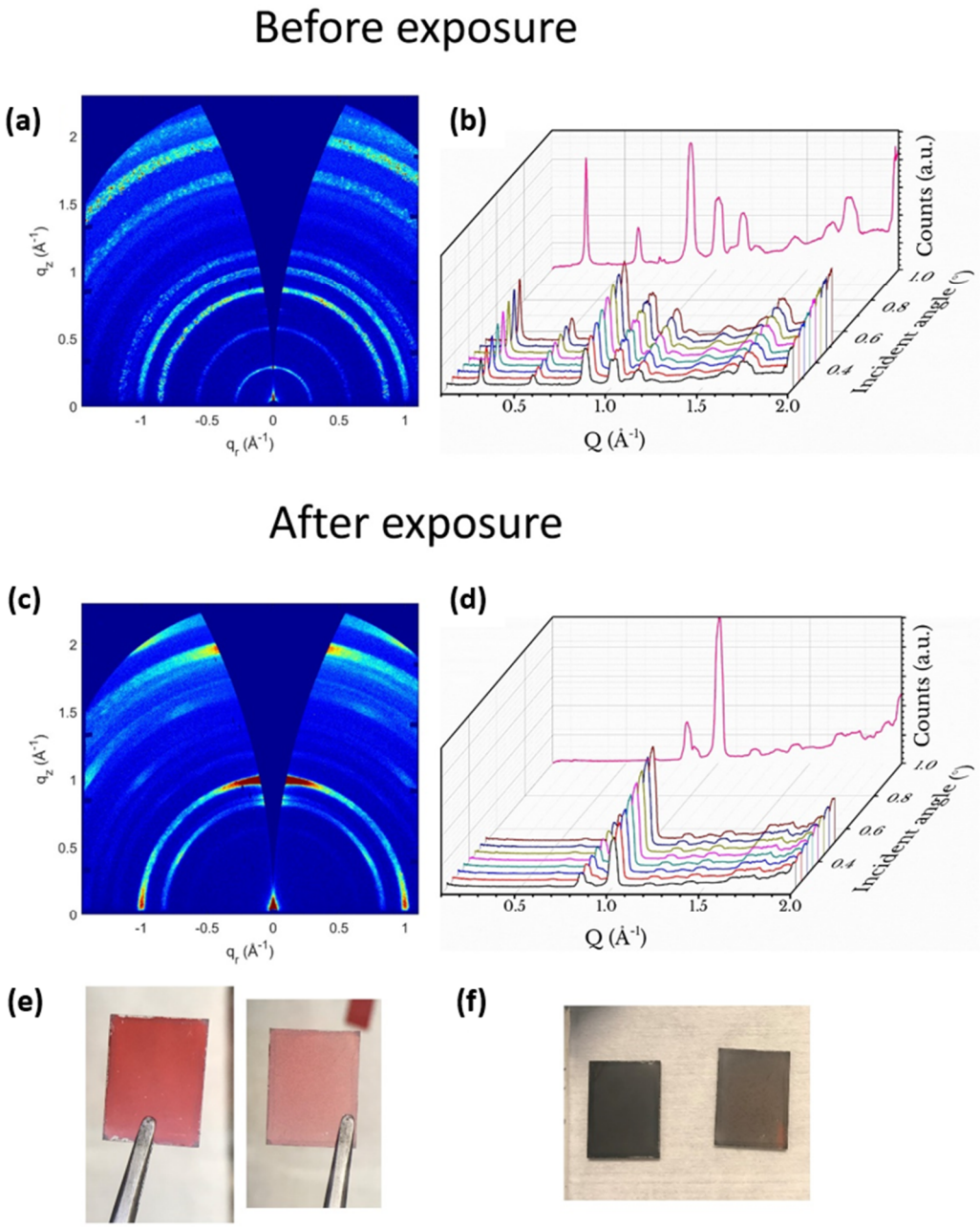

Figure S5: GIWAXS patterns at 0.32° incidence angle (defined as the angle between the grazing X-ray beam and the sample surface) of perovskite films (a) 4:1 air annealed and (c) 4:1 air annealed after exposure to high humidity. The x and y axis are the scattering vectors in the xy (Q_{xy}) and in z (Q_z) planes respectively. Here the main peaks observed after exposure to moisture are the Q ≈ 1 Å^{-1} $MAPbI_3$ (110), a small peak at Q ≈ 0.88 Å^{-1} (PbI_2) and another at Q ≈ 0.83 Å^{-1}. The final peak coincides with another peak previously attributed to LDPs reported by Song *et al.,* [3] and also lies in the expected region for both mono- and di-hydrate perovskite phases.[4] Radially integrated depth profiles of scattering peaks through (b) 4:1 before and (d) 4:1 after moisture exposure through a range of grazing incidence angles from 0.24° to 1°. Here, the composition appears comparable throughout the probed depth and all peaks increase in intensity at larger incidence angles. (e) 3.5:1 (left) and 4:1 (right) samples on quartz before exposure and (f) after exposure to high humidity of 3.5:1 (left) and 4:1 (right).

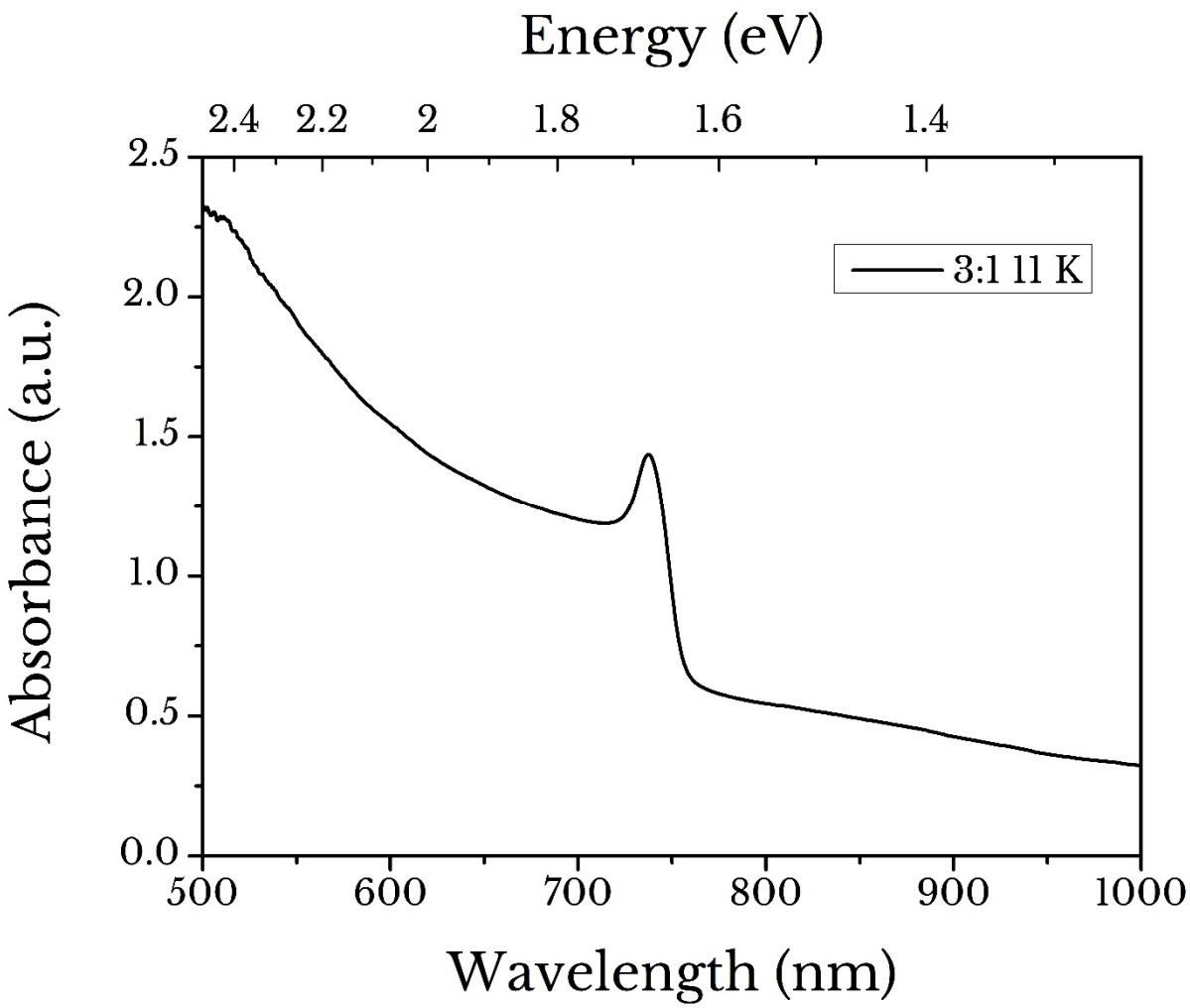

Figure S6: The absorption spectrum taken from a 3:1 (MAI:$PbCl_2$) perovskite film recorded at 11 K. Note the absence of any resolvable peaks for $\lambda < 700$ nm.

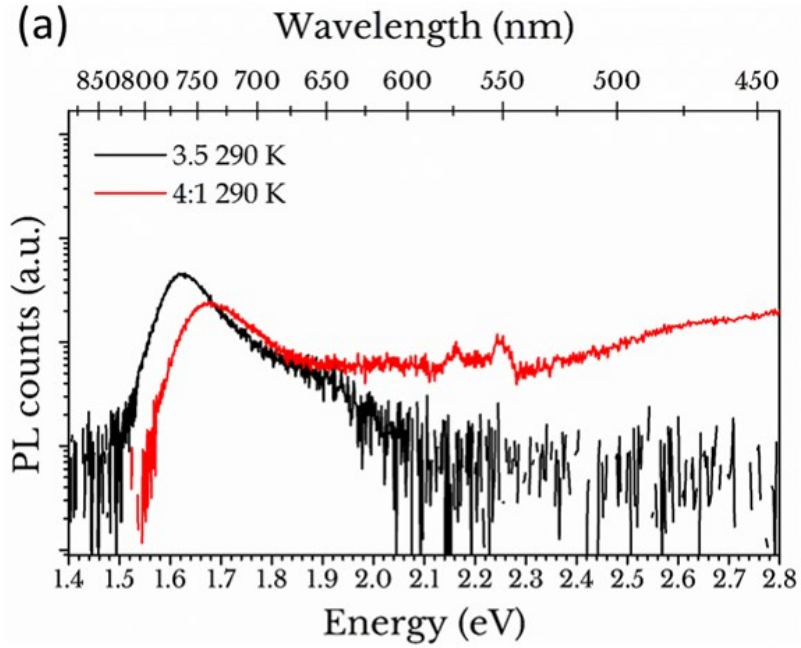

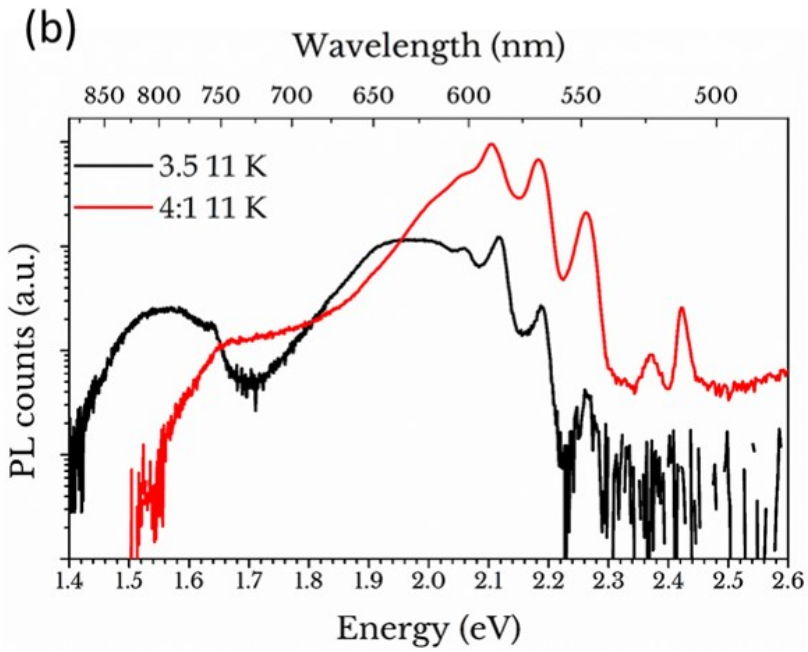

Figure S7: PL emission spectra for air annealed 3.5:1 (black) and N_2 glovebox annealed 4:1 (red) samples at (a) 290 K and (b) 11 K prepared on quartz. When plotted on a log-scale, some emission from LDP states is detected at room temperature at 545 and 565 nm from the glovebox annealed 4:1 sample. At low temperature, there is an order of magnitude greater LDP emission intensity from GB 4:1 compared to air 3.5:1, with peaks at 510, ~520-525 (only seen on this scale), 545, 565 and 585 nm. Both effects result from enhanced phase purity (more LDP than 3D) from the solution stoichiometry and GB annealing process.

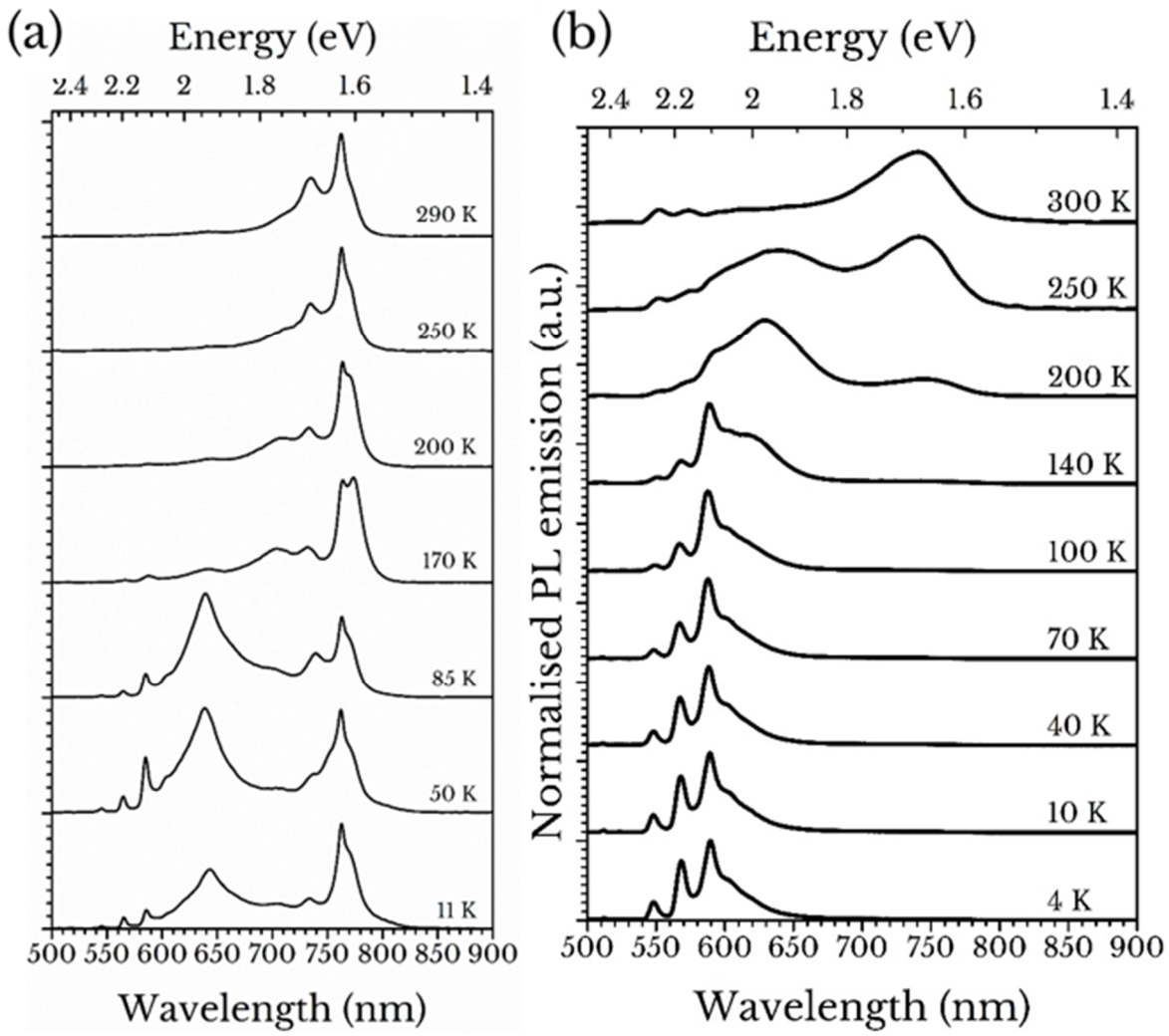

Figure S8: Temperature-dependant photoluminescence emission series for a) 3.5:1 air annealed film on hole-quenching ITO/PEDOT:PSS substrate and b) 4:1 air annealed film. For part a), the same material and series on quartz glass substrate is shown in Figure 3d. In this case, the emissive perovskite peak ≈770 nm does not broaden possibly due to the effect of holes being quenched from the material, reducing trap assisted recombination. [5] For part b), intensities are normalised and the low intensity emission at long wavelengths (at higher temperatures) is due to partial conversion in air.

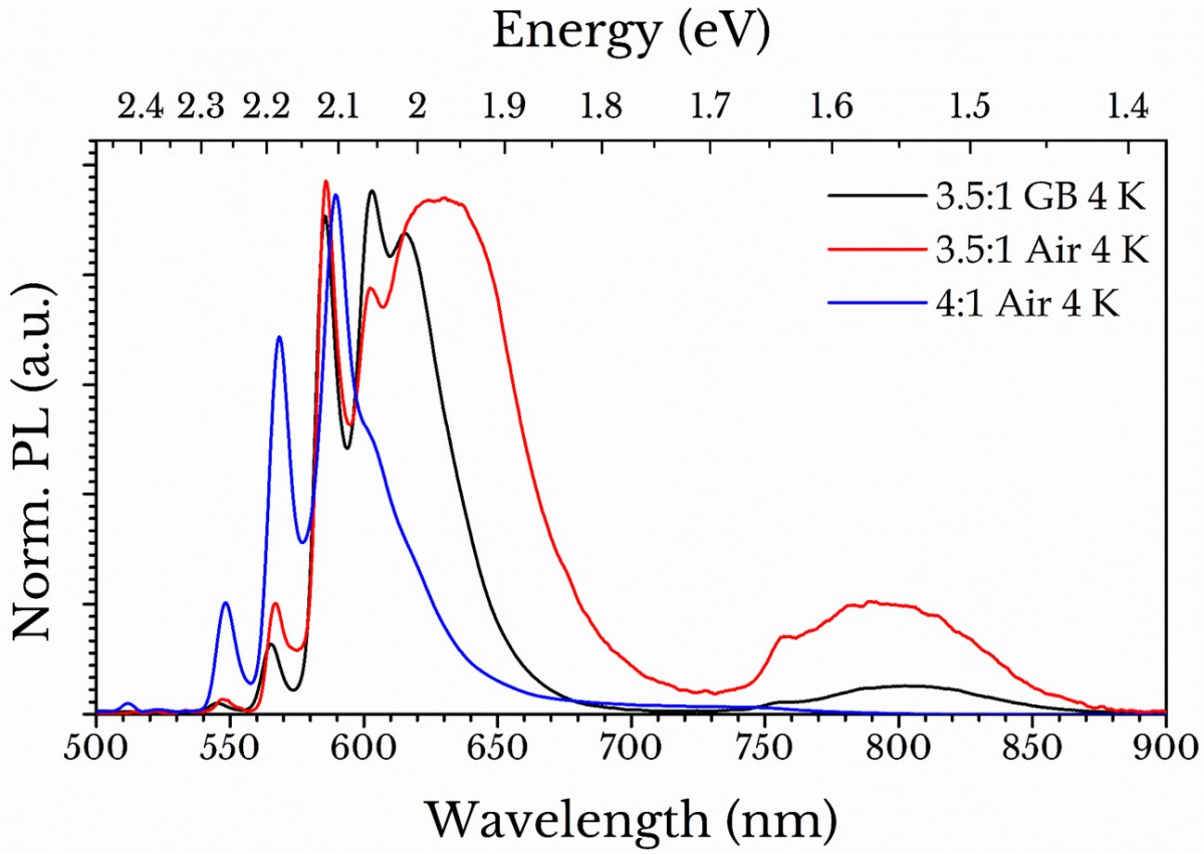

Figure S9: Low-temperature photoluminescence of 3.5:1 and 4:1 excess MAI perovskite films. Emission spectra of encapsulated films are shown deposited on ITO/PEDOT:PSS and annealed in air (red + blue lines) or in the glovebox (black). The glovebox annealed sample has reduced emission at around 640 nm and more defined emissive peaks are detected at 605 and 625 nm. For the 4:1 (blue) 3D emission is not detectable and there is a small red-shift observed for the LDP emission peaks.

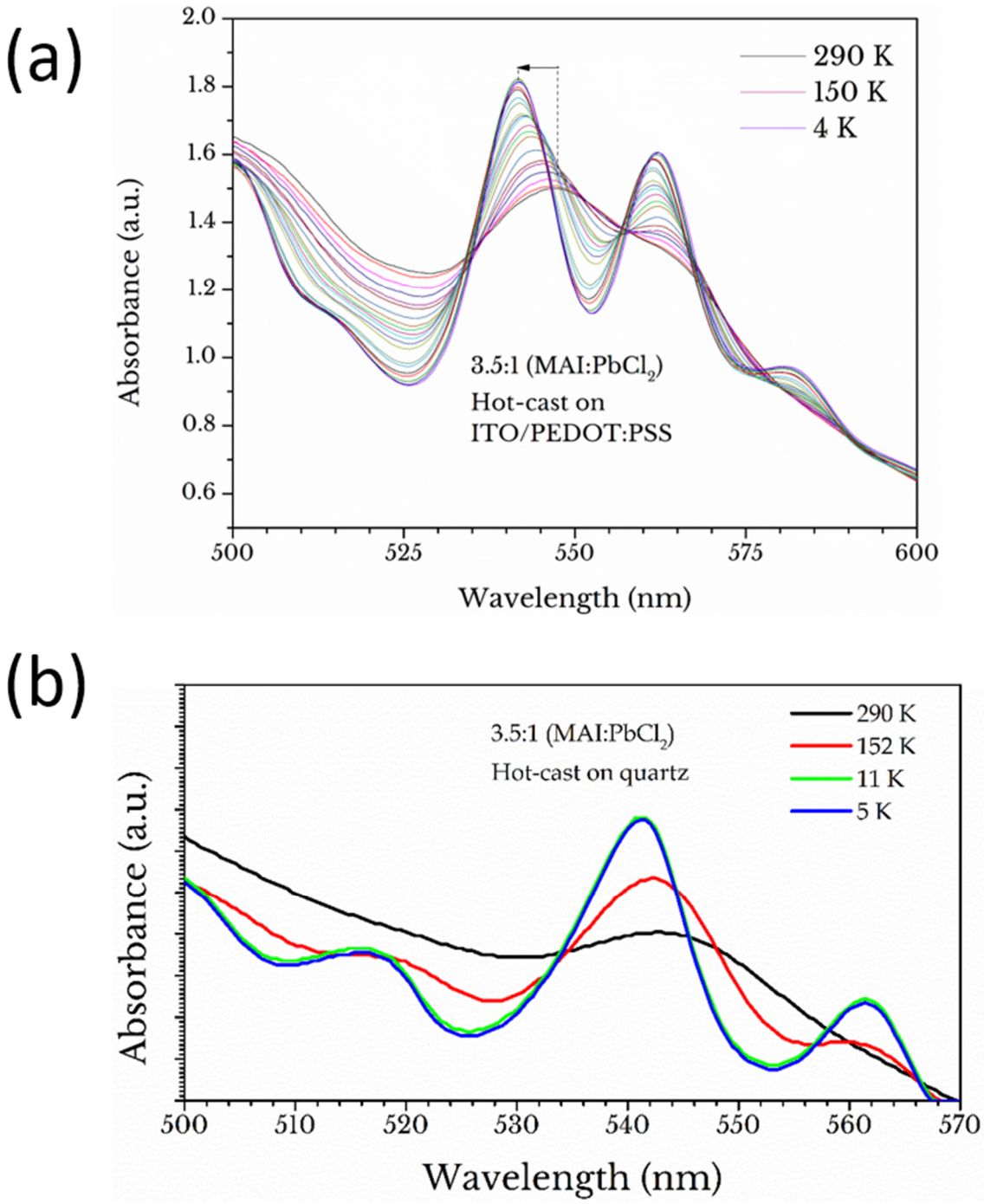

Figure S10: Emergence of low dimensional absorption features at low temperature. (a) The absorption band transition between 290 and 4 K with adjacent lines taken at intervals of 10 K illustrates the emergence of 2 clear excitonic features at 4 K on a 3.5:1 sample on ITO/PEDOT:PSS. (b) A similar trend is shown on a quartz glass substrate.

References

[1] C. M. M. Soe, C. C. Stoumpos, M. Kepenekian, B. Traoré, H. Tsai, W. Nie, B. Wang, C. Katan, R. Seshadri, A. D. Mohite, J. Even, T. J. Marks, M. G. Kanatzidis, *J. Am. Chem. Soc.* **2017**, *139*, 16297.

[2] K. Momma, F. Izumi, *J. Appl. Crystallogr.* **2011**, *44*, 1272.

[3] Z. Song, S. C. Watthage, A. B. Phillips, B. L. Tompkins, R. J. Ellingson, M. J. Heben, *Chem. Mater.* **2015**, *27*, 4612.

[4] A. Leguy, Y. Hu, M. Campoy-Quiles, M. I. Alonso, O. J. Weber, P. Azarhoosh, M. Van Schilfgaarde, M. T. Weller, T. Bein, J. Nelson, P. Docampo, P. R. F. Barnes, .

[5] D. Meggiolaro, S. Motti, E. Mosconi, A. barker, J. Ball, C. A. R. Perini, F. Deschler, A. Petrozza, F. De Angelis, *Energy Environ. Sci.* **2018**, *11*, 702.